THE JOURNAL OF BIOLOGICAL CHEMISTRY VOL. 290, NO. 8, pp. 4981–4993, February 20, 2015

A New Role for Annexin A11 in the Early Secretory Pathway via Stabilizing Sec31A Protein at the Endoplasmic Reticulum Exit Sites (ERES)*[S]

Received for publication, June 29, 2014, and in revised form, December 8, 2014 Published, JBC Papers in Press, December 24, 2014, DOI 10.1074/jbc.M114.592089

Hideki Shibata[‡1], **Takashi Kanadome**[‡2], **Hirofumi Sugiura**[‡], **Takeru Yokoyama**[‡], **Minami Yamamuro**[‡], **Stephen E. Moss**[§], **and Masatoshi Maki**[‡]

From the [‡]*Department of Applied Molecular Biosciences, Graduate School of Bioagricultural Sciences, Nagoya University, Furo-cho, Chikusa-ku, Nagoya 464-8601, Japan and the* [§]*Department of Cell Biology, UCL Institute of Ophthalmology, University College London, 11-43 Bath Street, London EC1V 9EL, United Kingdom*

Background: Apoptosis-linked gene 2 (ALG-2) is a calcium-dependent adaptor protein that is recruited to the Sec31A-positive ERES.
Results: Physical association between annexin A11 and Sec31A is mediated by ALG-2, and annexin A11 is required for stable association of Sec31A at the ERES.
Conclusion: Annexin A11 participates in ER-to-Golgi trafficking.
Significance: Annexin A11 is the first annexin shown to modulate the early secretory pathway.

Exit of cargo molecules from the endoplasmic reticulum (ER) for transport to the Golgi is the initial step in intracellular vesicular trafficking. The coat protein complex II (COPII) machinery is recruited to specialized regions of the ER, called ER exit sites (ERES), where it plays a central role in the early secretory pathway. It has been known for more than two decades that calcium is an essential factor in vesicle trafficking from the ER to Golgi apparatus. However, the role of calcium in the early secretory pathway is complicated and poorly understood. We and others previously identified Sec31A, an outer cage component of COPII, as an interacting protein for the penta-EF-hand calcium-binding protein ALG-2. In this study, we show that another calcium-binding protein, annexin A11 (AnxA11), physically associates with Sec31A by the adaptor function of ALG-2. Depletion of AnxA11 or ALG-2 decreases the population of Sec31A that is stably associated with the ERES and causes scattering of juxtanuclear ERES to the cell periphery. The synchronous ER-to-Golgi transport of transmembrane cargoes is accelerated in AnxA11- or ALG-2-knockdown cells. These findings suggest that AnxA11 maintains architectural and functional features of the ERES by coordinating with ALG-2 to stabilize Sec31A at the ERES.

After newly synthesized membrane and secretory proteins are correctly folded in the endoplasmic reticulum (ER),[3] they are incorporated into ER-derived transport vesicles to reach their final destinations, including the Golgi apparatus, endosomes, lysosomes, and the cell surface. Cargo protein sorting and vesicle formation are accomplished by the coat protein complex II (COPII) machinery at specialized, long lived subregions of the ER, termed ER exit sites (ERES) or transitional ER (1, 2). The COPII coat components and their essential regulators were first identified in yeast and are conserved from yeast to humans (3, 4). The coat consists of a small GTPase, Sar1, and two cytosolic protein complexes, Sec23-Sec24 and Sec13-Sec31. Sec31 interacts directly with Sar1 and Sec23, and the Sec13-Sec31 complex is polymerized into a polyhedral cage structure to form the functional outer coat that drives vesicle formation (5–7).

Release of calcium (Ca^{2+}) from the ER is an important signal for the control of multiple cellular processes (8). The role of Ca^{2+} as an essential factor in protein transport from the ER to Golgi apparatus was first reported by Beckers and Balch (9), who used semi-intact cells that reconstitute transport between organelles, to demonstrate that the Ca^{2+} chelator EGTA inhibits the ER-to-Golgi transport of the newly synthesized temperature-sensitive variant of vesicular stomatitis virus glycoproteins (tsO45 VSV-G). Subsequently, Ca^{2+} has been reported to be indispensable for VSV-G transport from the pre-Golgi intermediate compartments to the Golgi apparatus (10–12). In contrast, transport from the ER to the pre-Golgi was inhibited not by Ca^{2+} chelators but by treatment of semi-intact cells with elevated Ca^{2+} (10). To understand the complex effects of Ca^{2+} in the early stage of ER-to-Golgi transport, it was essential to identify Ca^{2+}-binding proteins that function in the early secretory pathway (13). We and others reported that the penta-EF-

* This work was supported in part by the Uehara Memorial Foundation (to H. S.), the Toyoaki Scholarship Foundation (to H. S.), Grant-in-aid for Scientific Research (C) 24580138 (to H. S.), and Grant-in aid for Scientific Research (B) 23380056 (to M. M.) from the Ministry of Education, Culture, Sports, Science, and Technology of Japan.
[S] This article contains supplemental Movies S1–S3.
[1] To whom correspondence should be addressed. E-mail: shibabou@agr.nagoya-u.ac.jp.
[2] Recipient of Japan Society for the Promotion of Science Research Fellowship for Young Scientists (DC1).
[3] The abbreviations used are: ER, endoplasmic reticulum; ABS, ALG-2-binding site; AnxA11, annexin A11; COPII, coat protein complex II; Endo H, endoglycosidase H; ERES, endoplasmic reticulum exit site; ERGIC, endoplasmic reticulum-Golgi intermediate compartment; FRAP, fluorescence recovery after photobleaching; VSV-G, vesicular stomatitis virus glycoprotein; RFP, red fluorescent protein; ANOVA, analysis of variance; IRES, internal ribosomal entry site.

hand protein ALG-2 binds Sec31A in a Ca^{2+}-dependent manner and is recruited to the Sec31A-positive ERES (14–16). Although Bentley *et al.* (17) showed that recombinant ALG-2 inhibited homotypic COPII vesicle fusion *in vitro*, the precise role of ALG-2 is unclear in the context of COPII function in living cells.

ALG-2 undergoes conformational changes upon binding of Ca^{2+} (18) and interacts in a Ca^{2+}-dependent fashion with multiple proteins (see Ref. 19 and references therein). ALG-2 exists as a homodimer or a heterodimer with peflin (20). It has been proposed that the ALG-2 dimer functions as a Ca^{2+}-dependent adaptor by bridging two interacting proteins (21, 22). In this study, we show that ALG-2 couples annexin A11 (AnxA11) with Sec31A. AnxA11 is a member of the family of vertebrate annexins that are Ca^{2+}-dependent phospholipid-binding proteins. AnxA11 has been implicated in nuclear envelope dynamics during prophase and in midbody formation during cytokinesis (23, 24). However, the role of AnxA11 in interphase remains unknown. The ALG-2-mediated physical association of AnxA11 with Sec31A prompted us to examine the role of AnxA11 in the early secretory pathway. We demonstrate here that AnxA11 is essential for the stable association of Sec31A with the ERES and for juxtanuclear positioning of the ERES in human fibrosarcoma HT1080 cells. Furthermore, siRNA-mediated silencing of ALG-2 or AnxA11 resulted in impaired integrity of the early secretory pathway.

EXPERIMENTAL PROCEDURES

Antibodies—Rabbit polyclonal antibodies against ALG-2 and ALIX and a goat polyclonal antibody against ALG-2 were prepared as described previously (14, 19). Rabbit polyclonal antisera against Sec31A and a mouse monoclonal antibody against p125 were kindly provided by Dr. Katsuko Tani, Tokyo University of Pharmacy and Life Science, Japan (25, 26). Other antisera against human Sec31A were raised in rabbits using the Sec31A C-terminal domain (1093–1220 amino acids) (Sec31A C terminus) fused with GST as an antigen, and specific antibodies were affinity-purified using Sec31A C terminus fused with maltose-binding protein. Rabbit polyclonal antibodies against Sec16A (A300-648A; Bethyl Laboratories, Montgomery, TX), RFP (R10367; Invitrogen), mouse monoclonal antibodies against GAPDH (clone MAB374; CHEMICON International, Temecula, CA), Strep tag (StrepMAB-Immo; IBA, Göttingen, Germany), and horseradish peroxidase (HRP)-conjugated rabbit polyclonal antibody against GFP (598-7; MBL, Nagoya, Japan) were obtained commercially. Goat polyclonal antibodies against AnxA11 (N-17, sc-9321 and L-19, sc-9322) and caspase-1 (C-15, sc-1780) were purchased from Santa Cruz Biotechnology (Santa Cruz, CA). Mouse monoclonal antibodies against Sec31A (clone 32), GM130 (clone 35), and AnxA11 (clone 16) were from BD Transduction Laboratories (San Jose, CA). Mouse monoclonal antibody against γ-tubulin (clone GTU-88) and rabbit polyclonal antibodies against ERGIC-53/p58 (E1031) and AnxA11 (HPA027545) were purchased from Sigma. HRP-conjugated goat antibodies against mouse IgG and rabbit IgG and HRP-conjugated rabbit antibody against goat IgG were purchased from Jackson ImmunoResearch (West Grove, PA). For immunostaining, we used AlexaFluor488-conjugated donkey antibody against mouse IgG, AlexaFluor488-conjugated donkey antibody against goat IgG, AlexaFluor555-conjugated donkey antibody against rabbit IgG, AlexaFluor647-conjugated donkey antibody against mouse IgG, AlexaFluor647-conjugated donkey antibody against rabbit IgG, and AlexaFluor647-conjugated donkey antibody against goat IgG (Invitrogen).

Plasmid Construction—Retroviral vectors encoding Sec31A C-terminally fused with SGFP2 (pCX4bsr/Sec31A-SGFP2) and a short hairpin RNA against ALG-2 (pshRNA$^{ALG\text{-}2}$) were described previously (14, 27). An siRNA target region in the firefly luciferase gene (5′-GCACTCTGATTGACAAATA-3′) was chosen (28), and oligonucleotides were annealed and cloned into pSUPER.retro.puro (OligoEngine, Seattle, WA). The vector is referred to as pshRNA^{Luc}. Constructs of pcDNA3/ALG-2 RNAi^{R} and pcDNA3/ALG-2$^{\Delta GF122}$ RNAi^{R} that express RNAi-resistant ALG-2 mRNAs were described previously (29). An internal ribosomal entry site (IRES) sequence derived from the encephalomyocarditis virus and a cDNA encoding TagRFP-T were amplified from pCX4bsr/SGFP2-ALG-2 and pAnxA11-TagRFP-T by PCR with the following pairs of oligonucleotides with an XhoI site (underlined): 5′-ACCGTCGACCTCGAGAACTAACTTAAGCTAGCAACG-3′ (sense) and 5′-GTATTATCGTGTTTTTCAAAGG-3′ (antisense) for IRES; and 5′-AAAACACGATAATACCATGGTGTCTAAGGGCGAAG-3′ (sense) and 5′-AGATGCATGCTCGAGTGGTATGGCTGATTATGATC-3′ (antisense) for TagRFP-T. The DNA fragments obtained were subcloned into the XhoI site of the pcDNA3/ALG-2 RNAi^{R} or pcDNA3/ALG-2$^{\Delta GF122}$ RNAi^{R} using an In-Fusion Advantage PCR cloning kit (Clontech/Takara Bio, Otsu, Japan) to construct pcDNA3/ALG-2 RNAi^{R}/IRES/TagRFP-T and pcDNA3/ALG-2$^{\Delta GF122}$ RNAi^{R}/IRES/TagRFP-T. To construct pSTREP-Sec31A and pSTREP-Sec31A$^{\Delta ABS}$, an EcoRI/SmaI fragment from pFLAG-Sec31A or pFLAG-Sec31A$^{\Delta 839-851}$ (27) was inserted into the EcoRI/EcoRV site of pEXPR-IBA105-B (30), respectively. Construction of a retroviral vector encoding AnxA11 C-terminally fused with SGFP2 (pCX4pur/AnxA11-SGFP2) will be described elsewhere. A retroviral vector encoding the temperature-sensitive variant of vesicular stomatitis virus glycoprotein (tsO45-G) C-terminally fused with SGFP2 (pCX4pur/tsO45 G-SGFP2) was constructed by replacing the AnxA11-coding sequence of pCX4pur/AnxA11-SGFP2 with the tsO45 G-coding sequence of pmTFP1-VSV-G (Allele Biotechnology and Pharmaceuticals, San Diego) using the BglII and the BamHI site.

Cell Culture, Infection, and Plasmid Transfection—HT1080, HEK293 YS14 (a subcloned HEK293 cell line) (14), and HEK293/ALG-2_{KD} (an ALG-2 knockdown cell line) (21) were maintained in DMEM supplemented with 10 or 5% fetal bovine serum, 100 units/ml penicillin, and 100 μg/ml streptomycin at 37 °C under humidified air containing 5% CO_2. An amphotropic murine leukemia virus-packaging cell line, PLAT-A, was kindly provided by Dr. Toshio Kitamura (Institute of Medical Science, University of Tokyo). HT1080 cell lines expressing Sec31A C-terminally fused with SGFP2, tsO45 G C-terminally fused with SGFP2, and short hairpin RNAs against ALG-2 and firefly luciferase were established by infection with recombi-

nant retroviruses, as described previously (27). Cells were transfected with plasmid DNAs by using conventional calcium phosphate precipitation method for HEK293 and HEK293-derived cell lines and by using FuGENE 6 (Promega, Madison, WI) for HT1080 and HT1080-derived cell lines according to the manufacturer's instructions.

Transient siRNA-mediated Knockdown—The Dicer-substrate siRNA duplexes against human ALG-2 (target sequence: siALG-2.1, 5′-AGCAATAAAGGGAATGTTAGACGTG-3′; siALG-2.4, 5′-AAAGACAGGAGTGGAGTGATATCAG-3′) and human AnxA11 (target sequence: siAnxA11.1, 5′-GGACATCAGATCAGAGTATAAGCGG-3′; siAnxA11.2, 5′-GCACATCCGAGAATTAAACAGAGCC-3′) were obtained from Integrated DNA Technologies (Coralville, IA). For all experiments, the negative control siRNA NC1 (target sequence, 5′-CGTTAATCGCGTATAATACGCGTAT-3′) was employed. HT1080 cells or HT1080 cells stably expressing Sec31A-GFP or tsO45-G-GFP were transfected with 10 nM siRNA by using RNAiMAX (Invitrogen) according to the manufacturer's instructions. After 72 h, cells were subjected to FRAP analysis, harvested for immunoblotting, or fixed for immunofluorescence analysis.

Fluorescence Recovery after Photobleaching (FRAP) Analysis—FRAP was performed essentially as described previously (27). Briefly, cells were seeded into glass-bottomed dishes (Asahi Glass, Tokyo, Japan), and the medium was replaced with Leivobitz's L15 medium (Invitrogen) containing 10% fetal bovine serum. Fluorescence images were obtained using an Olympus FV1000-D laser scanning confocal microscope equipped with an IX81 microscope with a ×60, 1.35 numerical aperture (NA) oil-immersion objective (UPLSAPO60XO) (Olympus, Tokyo, Japan) and a stage incubator system (Tokai Hit, Fujinomiya, Japan). The stage was heated at 37 °C, and cells were imaged for <90 min on the microscope stage. SGFP2 was exited using the 488-nm line of an argon laser set at 0.2–0.5% transmission, and emission was collected using a bandpass filter set at 505–550 nm. The pinhole diameter was set for 3 Airy units. For each time-lapse series, an optical zoom of 1.5 was used, and images were acquired every 232 ms at 192 × 32 resolution. SGFP2-fused Sec31A proteins at the ERES were photobleached using the SIM scanner in tornado scan mode with the 488-nm line of argon laser set at 100% transmission for 7.5 ms. The bleached region was a circle of 11 pixels in diameter located in the perinuclear area. The fluorescence intensities within the bleached region and cell-free area (background) were measured using the Olympus FV10-ASW software. After background subtraction, the fluorescence intensity of the bleached region over time was normalized with the average fluorescence intensity of 10 frames before photobleaching and was plotted as a function of time. For quantitative analysis, independent normalized data from 30 cells expressing SGFP2-fused Sec31A were averaged and fitted to a two-phase exponential $F(t) = A_0 + A_1(1 - e^{-k_1 t}) + A_2(1 - e^{-k_2 t})$, where A_0 is the offset of the curve; A_1 and A_2 are the relative amplitudes of the recovery curve, and k_1 and k_2 are the rate constants of fluorescence recovery corresponding to dissociation rates from which $t_{1/2}$ values were determined, $t_{1/2} = \ln(2)/k$. The best fit parameters are as follows: $A_0 = 0.281$; $A_1 = 0.186$; $k_1 = 0.904$; $A_2 = 0.273$; and $k_2 = 0.112$. The k_1 and k_2 parameters were fixed in further global analysis of the data sets of knockdown cells. For exogenously ALG-2-expressing cells, independent normalized data from 17 cells expressing RFP were averaged and fitted as described above. The k_1 and k_2 parameters ($k_1 = 1.105$ and $k_2 = 0.129$) were fixed in further global analysis of the data sets of exogenously ALG-2-expressing cells. These analyses were achieved with Origin 8J software (OriginLab, Northampton, MA). The relative size of the immobile and mobile fractions was calculated as follows: immobile fraction $(1 - A_0 - A_1 - A_2)/(1 - A_0)$; fast mobile fraction, $A_1/(1 - A_0)$; slow mobile fraction, $A_2/(1 - A_0)$.

Strep Pulldown Analysis—HEK293 cells transfected with pSTREP-Sec31A or pSTREP-Sec31A$^{\Delta ABS}$ were washed and harvested with PBS (137 mM NaCl, 2.7 mM KCl, 8 mM Na_2HPO_4 and 1.5 mM KH_2PO_4, pH 7.4), suspended in lysis buffer (20 mM HEPES-NaOH, pH 7.2, 142.5 mM KCl, 1.5 mM $MgCl_2$) containing 0.5% Triton X-100, 10 μM EGTA, and protease inhibitors (3 μg/ml leupeptin, 0.1 mM Pefabloc, 1 μM pepstatin A, 1 μM E-64, 0.2 mM PMSF), and homogenized with a tight-fitting glass homogenizer. Cleared cell lysates obtained by centrifugation at 10,000 × *g* for 10 min were incubated with Strep-Tactin-Sepharose (IBA) at 4 °C for more than 6 h in the presence of either 100 μM $CaCl_2$ or 5 mM EGTA. After the beads were recovered by low speed centrifugation and washed twice with the lysis buffer containing 0.1% Triton X-100 and either 100 μM $CaCl_2$ or 5 mM EGTA, the bead-bound proteins (Strep pulldown products) were resolved with SDS-PAGE, transferred to polyvinylidene difluoride membranes (Immobilon-P; Millipore, Billerica, MA), and probed with specific antibodies essentially as described previously (31). Chemiluminescent signals were detected by a LAS-3000mini lumino-image analyzer (Fujifilm, Tokyo, Japan) using SuperSignal West Pico chemiluminescent substrate (Thermo Fisher Scientific, Rockford, IL).

Immunoprecipitation Analysis—For AnxA11 immunoprecipitation, cleared cell lysates of untransfected or transfected cells obtained as described above were incubated with a mixture of polyclonal antibodies against AnxA11 (N-17 and L-19, Santa Cruz Biotechnology) at 4 °C for 3 h in the presence of either 100 μM $CaCl_2$ or 5 mM EGTA. A polyclonal antibody against caspase-1 p20 (C-15, Santa Cruz Biotechnology) was used as a control antibody. Then the lysates were incubated overnight at 4 °C with Dynabeads Protein G (Novex, Invitrogen). The beads were collected using a magnet and washed twice with lysis buffer containing 0.1% Triton X-100 and either 100 μM $CaCl_2$ or 5 mM EGTA. The immunoprecipitated proteins were subjected to SDS-PAGE followed by Western blot analysis.

Immunofluorescence Analysis—Untreated or siRNA-treated cells cultured on coverslips were fixed with ice-cold 4% paraformaldehyde in 100 mM phosphate buffer, pH 7.4, for 1 h at 4 °C (except for staining for Sec16A and ERGIC-53), rinsed with 15 mM glycine in PBS (PBS-Gly), and permeabilized with 0.1% Triton X-100 in PBS-Gly for 5 min at room temperature. After rinsing with PBS-Gly, the samples were blocked with 0.1% gelatin in PBS (PBS-gelatin) for more than 30 min at room temperature and then incubated with the primary antibodies diluted in PBS-gelatin overnight at 4 °C or for 1 h at room tem-

perature. In the case of staining for Sec16A and ERGIC-53, cells were fixed with 4% paraformaldehyde in 100 mM phosphate buffer, pH 7.4, for 1 h at room temperature and then permeabilized with 0.1% Triton X-100 or 30 μg/ml digitonin in PBS-Gly for 5 min. The samples were rinsed with PBS-gelatin and then incubated with secondary antibodies diluted in PBS-gelatin for 30 min at room temperature. After extensive rinses, the samples were mounted in a Mowiol 4-88 (Calbiochem)-based mounting medium (32) and then observed with an Olympus FV1000-D laser-scanning confocal microscope equipped with an IX81 microscope with a ×60, 1.35 numerical aperture oil-immersion objective (UPLSAPO60XO). Image contrast (black and white levels) was adjusted in ImageJ software (National Institutes of Health, Bethesda) without gamma adjustment. Images were pseudocolored and merged. Immunofluorescence intensity was assessed by line scan analysis using ImageJ.

For quantification of ERES distribution, cells were immunostained with a monoclonal antibody against γ-tubulin and an antibody against Sec16A to detect centrosome and ERES, respectively. Cells with one centrosome positioned adjacent to the nucleus were selected, and Z-stacks of optical sections spanning the entire cell were captured. Each Z-stack was projected onto a single plane, and the distance from each ERES in the cell to the centrosome was measured using ImageJ. More than 15 selected cells from two independent siRNA treatment samples were analyzed. Statistical analysis was done by one-way analysis of variance (ANOVA), followed by Tukey's test.

For quantification of ERGIC-53 or tsO45-G-GFP distribution, cells were immunostained with a monoclonal antibody against GM130 and an antibody against ERGIC-53 (for ERGIC-53). The ratio of fluorescence intensity for ERGIC-53 or for tsO45-G-GFP in the GM130-positive area to that in whole cell was calculated from more than 16 cells in two independent siRNA treatment samples. Statistical analysis was done by one-way ANOVA, followed by Tukey's test.

tsO45 VSV-G Transport Assays—tsO45 VSV-G transport assays were performed essentially as described previously (26). HT1080 cells stably expressing tsO45 VSV-G fused with SGFP2 (tsO45-G-GFP) were transfected with siRNAs as described above and cultured for 48 h at 37 °C. The cells were further incubated for 24 h at 39 °C, and the medium was changed to pre-warmed (32 °C) Leivobitz's L15 medium containing 10% fetal bovine serum and 20 μg/ml cycloheximide. The cells were further incubated at 32 °C to allow tsO45-G-GFP transport from the ER. After incubation for the indicated times, the cells were fixed, and fluorescence images were obtained with a confocal microscope. Alternatively, cells were harvested at the indicated times, solubilized with 0.5% SDS and 40 mM dithiothreitol, and heated at 100 °C for 10 min. The lysate was digested with endoglycosidase H (New England Biolabs, Ipswich, MA) according to the manufacturer's instructions at 37 °C for more than 12 h, and then resolved by SDS-PAGE on 7% gels. The tsO45-G-GFP was visualized by immunoblotting with HRP-conjugated rabbit polyclonal antibody against GFP (MBL). The intensities of the immunoreactive bands were quantified using ImageJ. Statistical analysis was performed using one-way ANOVA, followed by Tukey's test.

RESULTS

ALG-2 Regulates Sec31A Dynamics in Living Cells—To test a possible role of ALG-2 on Sec31A cycling between the cytosol and the ERES, we first established an HT1080 cell line stably expressing both SGFP2-fused Sec31A (Sec31A-GFP) and a short hairpin-type RNA (shRNA) targeting ALG-2 (Sec31A-gfp/ALG-2_{KD} cell). Cell lines expressing Sec31A-GFP without or with shRNA targeting firefly luciferase (Sec31A-gfp cell and Sec31A-gfp/Luc_{KD} cell, respectively) were used as control. In Western blot analysis, endogenous Sec31A proteins in parental cells were detected as four bands, probably due to alternative splicing, whereas the endogenous Sec31A proteins were decreased in the three cell lines (Sec31A-gfp, Sec31A-gfp/ALG-2_{KD}, and Sec31A-gfp/Luc_{KD} cells) (Fig. 1*A*). Instead, Sec31A-GFP proteins were detected as a single band with similar expression levels in the three cell lines. It has been previously reported that knockdown of Sec13 results in concomitant loss of Sec31 (33). Sec13 may therefore be preferentially occupied by Sec31A-GFP, leading to destabilization of endogenous Sec31A. ALG-2 proteins were decreased in Sec31A-gfp/ALG-2_{KD} cells compared with parental, Sec31A-gfp, and Sec31A-gfp/Luc_{KD} cells. As shown in Fig. 1*B*, the cytoplasmic punctate structures labeled with Sec31A-GFP in the three cell lines partially or completely overlap puncta labeled with an antibody against Sec16A, a key regulator of COPII vesicle formation in mammalian cells (34–37). Therefore these structures could be defined as *bona fide* ERES. To examine the effects of ALG-2 suppression on Sec31A dynamics, we performed fluorescence recovery after photobleaching (FRAP) analysis. In the FRAP, a region including the puncta labeled with Sec31A-GFP was photobleached, and then the recovery of GFP fluorescence was followed (Fig. 1*C*, supplemental Movie S1). The time-lapse images and the graph of relative fluorescence recovery over time indicate that the maximum recovery rate is higher in the Sec31A-gfp/ALG-2_{KD} cells than in the Sec31A-gfp and the Sec31A-gfp/Luc_{KD} cells. Relative averaged recovery rates after photobleaching in multiple cells are plotted as a function of time (Fig. 1*D*). Recovery kinetics of the control cells (Sec31A-gfp cells) fitted well with a two-component model, which predicts the presence of two mobile populations of Sec31A-GFP at the ERES with different binding constants as follows: a fast mobile population, $t_{1/2} = 0.77$ s, and a slow mobile population, $t_{1/2} = 6.21$ s. ALG-2 depletion significantly reduced the immobile Sec31A-GFP population to less than half, whereas the fast mobile population was increased. Thus, ALG-2 contributes to the stable association of Sec31A with the ERES structures in living cells.

Mouse and human ALG-2 have two alternatively spliced isoforms, which are transcribed in a ratio favoring the long isoform (designated here as ALG-2^{WT}) (38). The short minor isoform differs from ALG-2^{WT} by lacking Gly^{121} and Phe^{122} (designated here as ALG-$2^{\Delta GF122}$). In our *in vitro* binding assay, both isoforms can interact with Sec31A (14, 29, 31). To explore whether one or both isoforms of ALG-2 function in the Sec31A dynamics, ALG-2^{WT} and ALG-$2^{\Delta GF122}$ were expressed in Sec31A-gfp/ALG-2_{KD} cells (Fig. 2*A*). In the rescue experiment, we used expression plasmids bearing an RNAi-resistant cDNA of ALG-

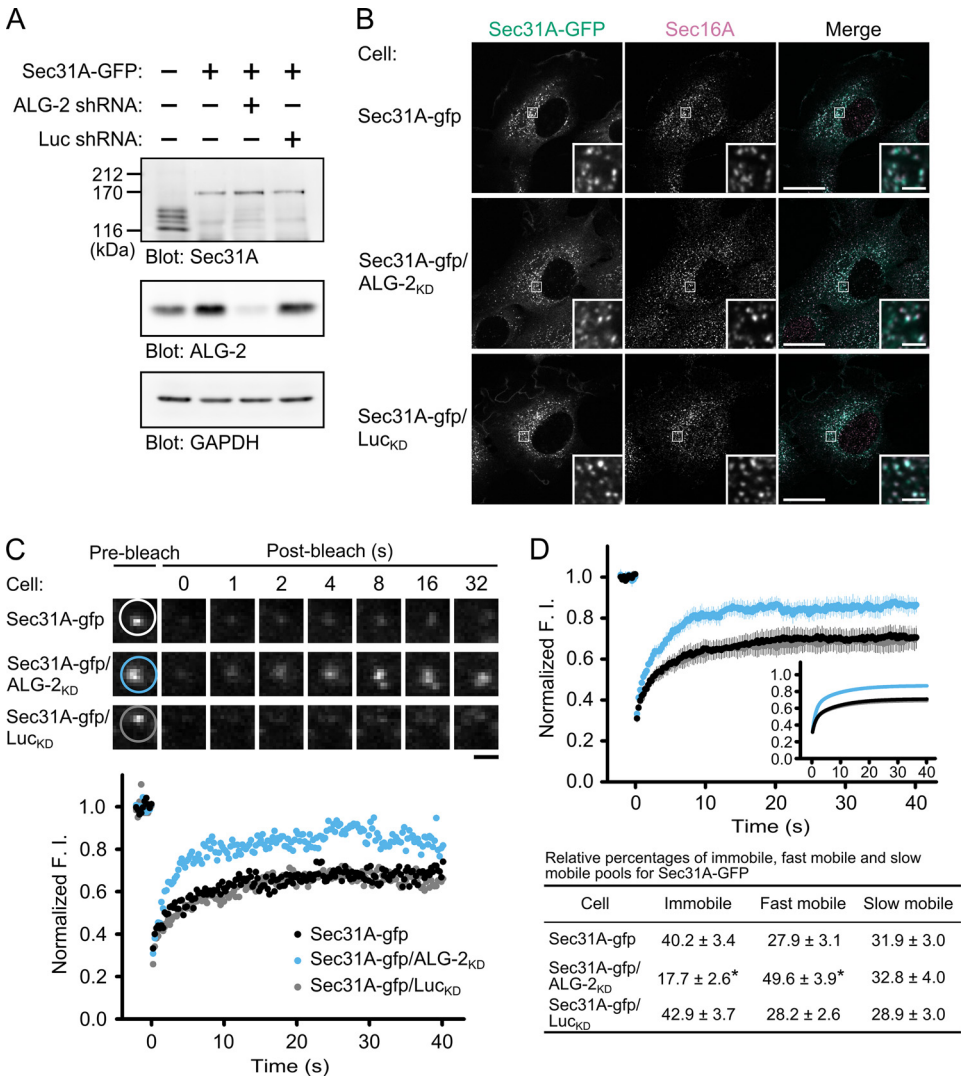

Relative percentages of immobile, fast mobile and slow mobile pools for Sec31A-GFP

Cell	Immobile	Fast mobile	Slow mobile
Sec31A-gfp	40.2 ± 3.4	27.9 ± 3.1	31.9 ± 3.0
Sec31A-gfp/ALG-2_{KD}	17.7 ± 2.6*	49.6 ± 3.9*	32.8 ± 4.0
Sec31A-gfp/Luc_{KD}	42.9 ± 3.7	28.2 ± 2.6	28.9 ± 3.0

FIGURE 1. **Effects of ALG-2 knockdown on Sec31A dynamics in living cells.** *A,* immunoblots of proteins from HT1080 cells stably expressing SGFP2-fused Sec31A (*Sec31A-GFP*) with or without short hairpin-type RNA target for human ALG-2 (*ALG-2 shRNA*) or firefly luciferase (*Luc shRNA*). Cell lysates from the parental and stable cells were prepared and immunoblotted with the indicated antibodies. *B,* confocal micrographs of Sec31A-gfp, Sec31A-gfp/ALG-2_{KD}, and Sec31A-gfp/Luc_{KD} cells labeled with an antibody against Sec16A. Cells were fixed with 4% paraformaldehyde in phosphate buffer for 1 h at room temperature, permeabilized with 0.1% Triton X-100, and then stained with an antibody against Sec16A. The *right panel* in each row shows merged images with the pseudocolors: *green* (Sec31A-GFP) and *magenta* (Sec16A). *The lower right insets* are magnified views of the *white squares*. *Scale bars,* 20 μm and 2 μm (*inset*). *C,* representative FRAP experiments from Sec31A-gfp, Sec31A-gfp/ALG-2_{KD}, and Sec31A-gfp/Luc_{KD} cells. Each region indicated by *white, light blue,* and *gray circles* in *upper panels* was photobleached, and fluorescence recovery was followed and plotted over time (*lower graph*). *Scale bar,* 1 μm. The corresponding supplemental movie S1 is shown in the supplemental material. *D,* quantitative FRAP analysis of Sec31A-GFP in Sec31A-gfp, Sec31A-gfp/ALG-2_{KD}, and Sec31A-gfp/Luc_{KD} cells. Normalized mean recovery rate after photobleaching for Sec31A-GFP of Sec31A-gfp cells (*black,* $n = 25$), Sec31A-gfp/ALG-2_{KD} cells (*light blue,* $n = 20$), and Sec31A-gfp/Luc_{KD} cells (*gray,* $n = 28$) is plotted. *Error bars* represent the 95% confidence intervals. The *inset* shows fits to a two-phase exponential equation (*upper panel*). Individual relative sizes of the immobile and mobile fractions (fast mobile fraction and slow mobile fraction) were calculated and described as means ± S.E. in the *lower table*. The statistical significance of differences was analyzed by one-way ANOVA, followed by Tukey's test. *Asterisks* indicate a statistically significant difference ($p < 0.05$).

2^{WT} or ALG-$2^{\Delta GF122}$, an IRES sequence, and a TagRFP-T cDNA to distinguish transfected cells from untransfected cells. Indirect immunofluorescence analysis using antibody against ALG-2 showed that TagRFP-T-positive cells concomitantly express the ALG-2 isoforms in the Sec31A-gfp/$ALG2_{KD}$ cells transfected with pALG-2^{WT}/IRES/RFP or pALG-$2^{\Delta GF122}$/IRES/RFP. In the FRAP analysis (Fig. 2, *B* and *C,* and supplemental Movie S2), expression of ALG-2^{WT} resulted in restoration of the immobile population, whereas the recovery kinetics of Sec31A-GFP after photobleaching was similar between ALG-$2^{\Delta GF122}$-expressing cells and control cells expressing only TagRFP-T. These results suggest that the major isoform of ALG-2 is responsible for stable association of Sec31A with the ERES structures.

ALG-2 Mediates the Physical Association of Annexin A11 with Sec31A—Why does ALG-2^{WT}, but not ALG-$2^{\Delta GF122}$, rescue the stabilization of Sec31A at the ERES, even though both isoforms interact with Sec31A? We speculated that ALG-2^{WT} recruits a specific binding protein to the ERES by its adaptor function (22). In our *in vitro* binding analysis, recombinant ALG-2^{WT} directly bound to various proteins with different affinities (19). Among them, annexin A11 (AnxA11) has a long N-terminal regulatory region that shows a strong interaction with ALG-2^{WT} (39). To examine whether AnxA11 forms a

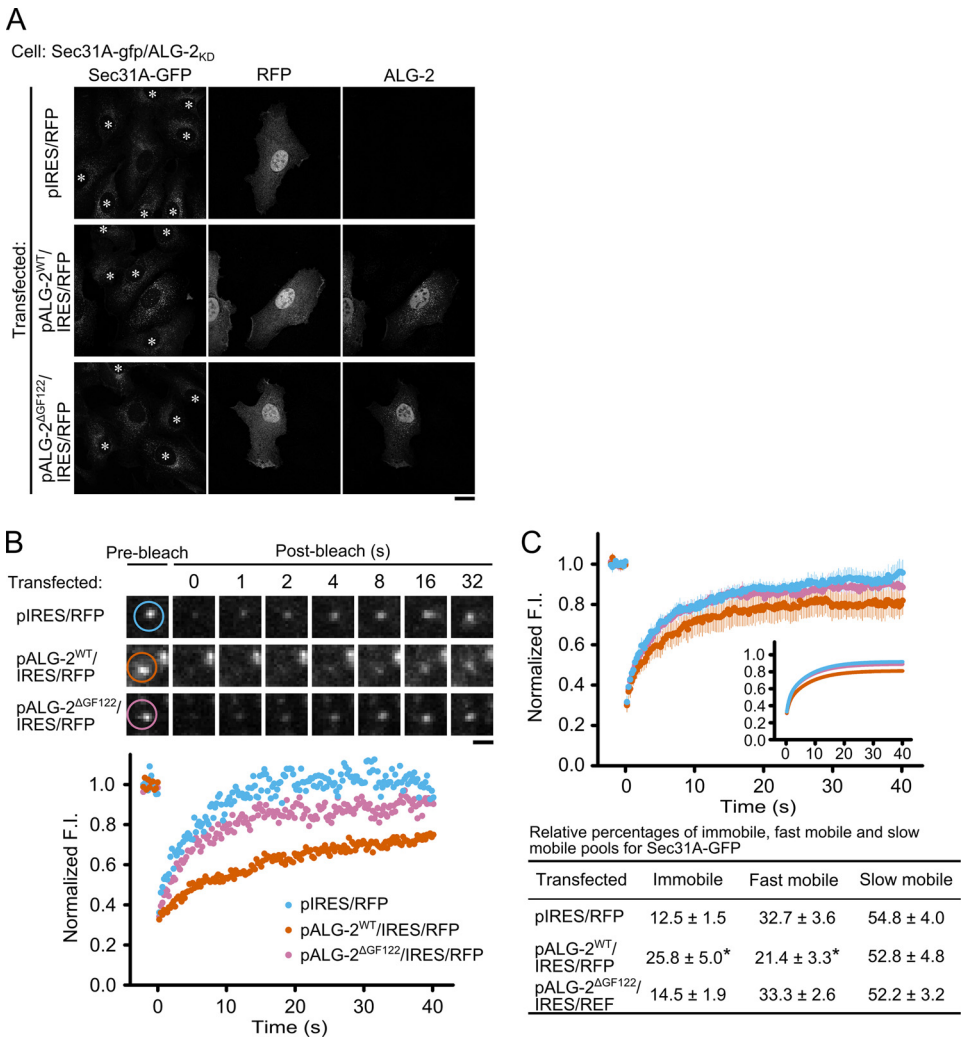

Relative percentages of immobile, fast mobile and slow mobile pools for Sec31A-GFP

Transfected	Immobile	Fast mobile	Slow mobile
pIRES/RFP	12.5 ± 1.5	32.7 ± 3.6	54.8 ± 4.0
pALG-2^{WT}/IRES/RFP	25.8 ± 5.0*	21.4 ± 3.3*	52.8 ± 4.8
pALG-2$^{\Delta GF122}$/IRES/REF	14.5 ± 1.9	33.3 ± 2.6	52.2 ± 3.2

FIGURE 2. **Effects of ALG-2 rescue in the ALG-2 knockdown cells on Sec31A dynamics.** *A*, confocal micrographs of Sec31A-gfp/ALG-2_{KD} cells expressing ALG-2 isoforms together with Tag-RFP-T through IRES. Cells were transfected with indicated expression plasmids, followed by fixation with 4% paraformaldehyde in phosphate buffer on ice for 1 h and permeabilization with 0.1% Triton X-100. The cells were then double-stained with antibodies against RFP and ALG-2. *Asterisks* in the *left panels* indicate cells expressing no TagRFP-T. *Scale bar*, 20 μm. *B*, representative FRAP experiments of transfected Sec31A-gfp/ALG-2_{KD} cells with TagRFP-T signals. Cells were transfected with the indicated plasmids, and cells expressing TagRFP-T were then subjected to FRAP analysis. The region indicated by *light blue, orange,* and *magenta circles* in the *upper panels* was photobleached, and fluorescence recovery was followed and plotted over time (*lower graph*). *Scale bar*, 1 μm. The corresponding supplemental movie S2 is shown in the supplemental material. *C*, quantitative FRAP analysis of Sec31A-GFP in transfected Sec31A-gfp/ALG-2_{KD} cells. Normalized mean recovery rate after photobleaching for Sec31A-GFP of Sec31A-gfp/ALG-2_{KD} cells without rescue (*light blue*, $n = 17$), with ALG-2^{WT} rescue (*orange*, $n = 18$), and with ALG-$2^{\Delta GF122}$ rescue (*magenta*, $n = 21$) are plotted and analyzed as described in Fig. 1*D*. The individual relative size of the immobile and mobile fractions (fast mobile fraction and slow mobile fraction) were calculated and described as means ± S.E. in the *lower table*. The statistical significance of differences was analyzed by one-way ANOVA, followed by Tukey's test. *Asterisks* indicate a statistically significant difference ($p < 0.05$).

complex with Sec31A, we performed pulldown assays using HEK293 cells expressing Strep-tagged Sec31A (Strep-Sec31A) and a mutant of Sec31A that lacks the ALG-2-binding site (Strep-Sec31A$^{\Delta ABS}$) (Fig. 3*A*). Specific bands corresponding to endogenous ALG-2 were detected in the pulldown product of Strep-Sec31A in the presence of Ca^{2+} but not in the presence of EGTA. No ALG-2 bands were detected in the pulldown products of Strep-Sec31A$^{\Delta ABS}$ in either condition. However, AnxA11, but not ALIX, was detected in the pulldown product of Strep-Sec31A in the presence of Ca^{2+}. In contrast, AnxA11 was undetectable in the pulldown products of Strep-Sec31A$^{\Delta ABS}$. These results indicate that AnxA11 interacts with Sec31A in a Ca^{2+}-dependent manner and that the ALG-2-binding site in Sec31A is essential for the interaction. To investigate whether the interaction between AnxA11 and Sec31A occurs at endogenous cellular protein levels, we next performed a co-immunoprecipitation assay with anti-AnxA11 antibodies. The commercially available antibodies against the N-terminal region of AnxA11 immunoprecipitated endogenous AnxA11 in the presence and absence of Ca^{2+} with low efficiency (14.8 ± 4.0% input, $n = 3$), whereas both ALG-2 and Sec31A were co-immunoprecipitated with the anti-AnxA11 antibodies from cell lysates in the presence of Ca^{2+} (ALG-2, 6.6 ± 2.4% input; Sec31A, 0.25 ± 0.04% input) but not in the presence of EGTA (Fig. 3*B*, *left panels*). This indicates that the three proteins can exist as a physical Ca^{2+}-dependent complex in cells. In contrast, Sec31A was undetectable in the anti-AnxA11 immunoprecipitates from cells stably expressing a short hairpin RNA targeting ALG-2 even in the presence of Ca^{2+} (Fig. 3*B*, *right panels*). As shown in Fig. 3*C*, the requirement of ALG-2 for the

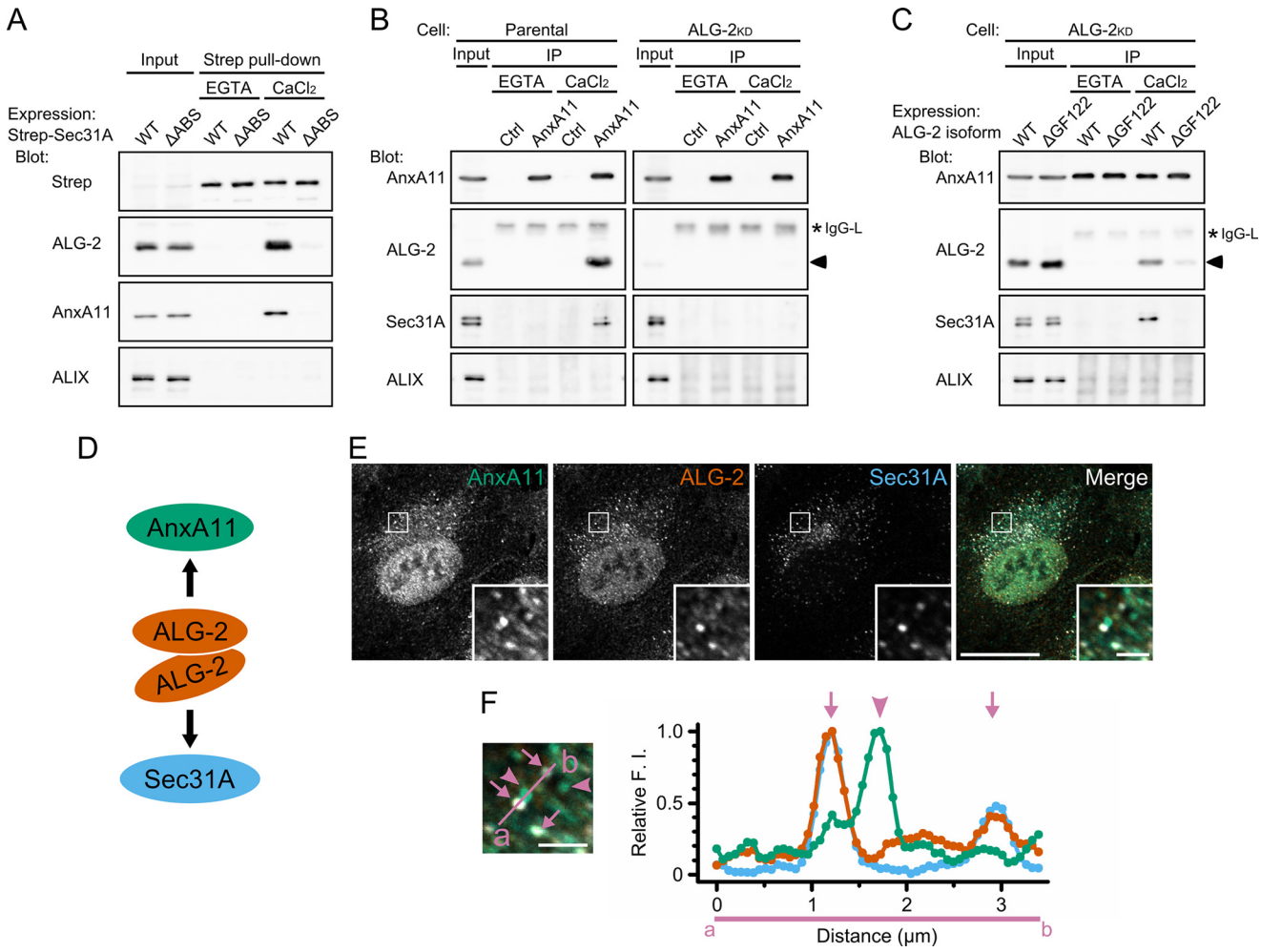

FIGURE 3. **ALG-2 calcium-dependently couples AnxA11 with Sec31A.** *A*, immunoblots of proteins in the Strep pulldown products from HEK293 cells expressing Strep-tagged Sec31A (WT) or its deletion mutant lacking the ALG-2-binding site (amino acids 839–851) (ΔABS). HEK293 cells transfected with pSTREP-Sec31A or pSTREP-Sec31A$^{\Delta ABS}$ were lysed, and cleared lysate (*Input*) was incubated with Strep-Tactin beads in the presence of 5 mM EGTA or 100 μM $CaCl_2$. After washing, pulldown products (*Strep pulldown*) were analyzed by Western blotting using indicated antibodies. The relative amount of cleared cell lysate proteins (*Input*) used for analysis of Strep pulldown products was 20% for Strep, 5% for ALG-2, and 0.5% for AnxA11 and ALIX. Representative data obtained from three independent experiments is shown. *B* and *C*, immunoblots of proteins in the immunoprecipitates (*IP*) with antibodies against AnxA11 from the cleared cell lysates of HEK293 cells (*Parental*) (*B*, *left panels*), ALG-2 knockdown HEK293 cells stably expressing short hairpin-type RNA target for ALG-2 (ALG-2_{KD}) (*B*, *right panels*), or ALG-2_{KD} cells transiently expressing either the major or the minor isoform of ALG-2 (WT or ΔGF122, respectively) (*C*). Cells were lysed, and cleared cell lysate (*Input*) was incubated first with polyclonal antibody against caspase-1 p20 (negative control, *Ctrl*) or polyclonal antibody against AnxA11 and then with magnetic beads carrying protein G in the presence of 5 mM EGTA or 100 μM $CaCl_2$. After washing, immunoprecipitates (*IP*) were analyzed by Western blotting using indicated antibodies. The relative amount of cleared cell lysate proteins (*input*) used for analysis of immunoprecipitation products was 10% for AnxA11, 3% for ALG-2, and 0.5% for Sec31A and ALIX. Representative data obtained from three (*B*, *left panel*, and *C*) and two (*B*, *right panel*) independent experiments are shown. *Arrowheads* and *asterisks* indicate ALG-2 and light chains of IgG, respectively. *D*, schematic representation of ALG-2-mediated physical association of AnxA11 with Sec31A. ALG-2^{WT} forms dimer and couples AnxA11 with Sec31A in a calcium-dependent manner. *E* and *F*, confocal micrographs of HT1080 cells stained with antibodies against AnxA11, ALG-2, and Sec31A. Cells were fixed with 4% paraformaldehyde in phosphate buffer on ice for 1 h, permeabilized with 0.1% Triton X-100, and then triple-stained with indicated antibodies. The *right panel* in *E* shows merged images with the pseudocolors as follows: *green* (AnxA11), *orange* (ALG-2), and *light blue* (Sec31A). The *lower right insets* are magnified view of the *white squares*. *Scale bars*, 20 μm and 2 μm (*inset*). *Left panel* in *F* is magnified image of *inset* from *right panel* in *E*. *Arrows* and *arrowheads* indicate AnxA11-positive puncta overlapping and nonoverlapping with ALG-2/Sec31A-positive structures, respectively. *Scale bar*, 2 μm. Fluorescence intensities along a line scan indicated in the *left panel* (from *a* to *b*) crossing Sec31A/ALG-2-positive puncta were measured by ImageJ, and relative fluorescence intensities are presented by *green* (AnxA11), *orange* (ALG-2), and *light blue* (Sec31A) in a *graph* (*F*, *right panel*), where the maximum value is 1.0.

Sec31A-AnxA11 interaction was confirmed by recovery of the immunoreactive band of Sec31A in the anti-AnxA11 immunoprecipitates with overexpression of ALG-2^{WT} (that binds both Sec31A and AnxA11), although there was no detectable band of Sec31A in the immunoprecipitates from cells overexpressing ALG-2$^{\Delta GF122}$ (that lacks the ability to bind AnxA11). These results clearly suggest that the major isoform of ALG-2 bridges between Sec31A and AnxA11 in a Ca^{2+}-dependent fashion (Fig. 3*D*). We next assessed by immunofluorescence analysis whether or not AnxA11 is localized to the ERES. In HT1080 cells, endogenous AnxA11 exists predominantly in the nucleus with additional punctate staining in the cytoplasm (Fig. 3*E*). A subset of the cytoplasmic puncta of AnxA11 indeed overlapped with both ALG-2 and Sec31A as shown by *arrows* in Fig. 3*F*. When fluorescence intensities along the line crossing the ALG-2/Sec31A-positive and -negative puncta of AnxA11 (indicated by *arrows* and *arrowheads*, respectively) were quantified, fluorescence intensities for AnxA11 in the ALG-2/Sec31A-positive

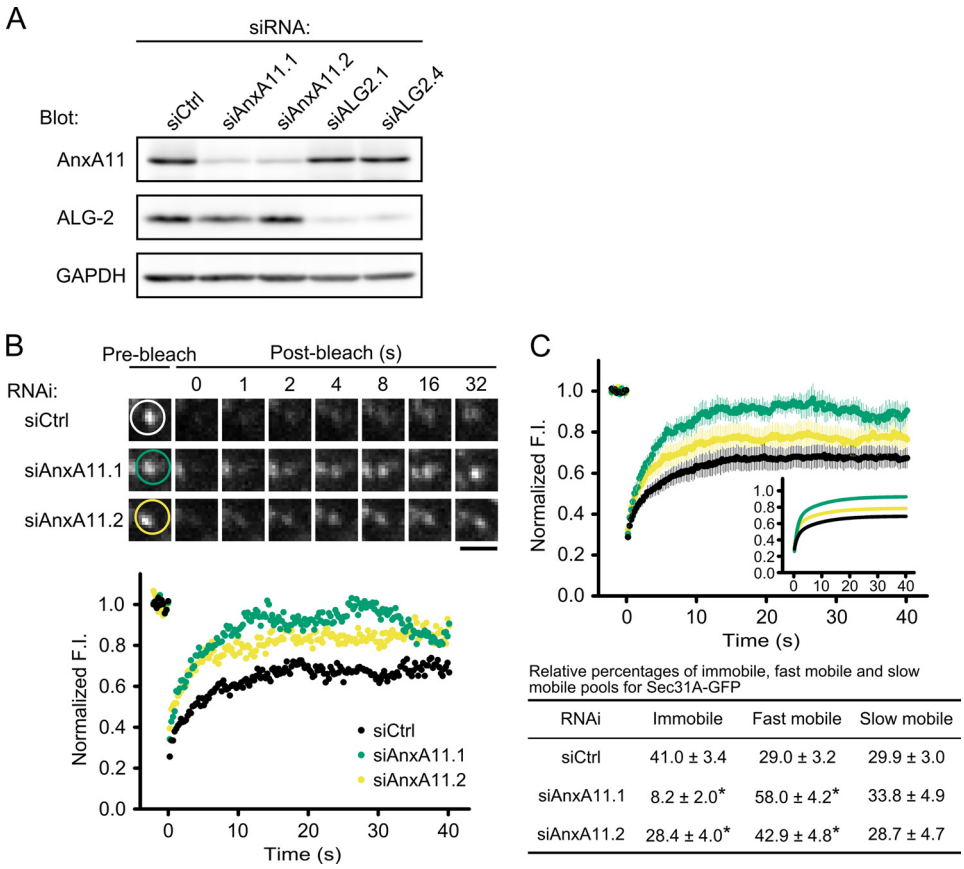

Relative percentages of immobile, fast mobile and slow mobile pools for Sec31A-GFP

RNAi	Immobile	Fast mobile	Slow mobile
siCtrl	41.0 ± 3.4	29.0 ± 3.2	29.9 ± 3.0
siAnxA11.1	8.2 ± 2.0*	58.0 ± 4.2*	33.8 ± 4.9
siAnxA11.2	28.4 ± 4.0*	42.9 ± 4.8*	28.7 ± 4.7

FIGURE 4. **Effect of AnxA11 knockdown on Sec31A dynamics in living cells.** *A,* immunoblots of proteins in HT1080 cells treated with indicated siRNAs. Cells transiently transfected with control (*siCtrl*), ALG-2 (*siALG-2.1* or *siALG-2.4*), or AnxA11 (*siAnxA11.1* or *siAnxA11.2*) siRNAs were lysed, and the cell lysates were analyzed by Western blotting with the indicated antibodies. *B,* representative FRAP experiments of Sec31A-GFP in Sec31A-gfp cells transfected with indicated siRNAs. Cells were transfected with control (*siCtrl*) or AnxA11 siRNAs (*siAnxA11.1* or *siAnxA11.2*) and then subjected to FRAP analysis. The region indicated by *white, green,* and *yellow circles* in *upper panels* was photobleached, and fluorescence recovery was followed and plotted over time (*lower graph*). *Scale bar,* 1 μm. The corresponding supplemental movie S3 is shown in the supplemental material. *C,* quantitative FRAP analysis of Sec31A-GFP in siRNA-treated Sec31A-gfp cells. Normalized mean recovery rate after photobleaching for Sec31A-GFP of Sec31A-gfp cells transfected with control siRNA (*black, n* = 27) and with AnxA11 siRNA (siAnxA11.1: *green, n* = 17; siAnxA11.2: *yellow, n* = 18) are plotted and analyzed as described in Fig. 1*D*. Individual relative sizes of the immobile and mobile fractions (fast mobile fraction and slow mobile fraction) were calculated and described as means ± S.E. in the *lower table*. The statistical significance of differences was analyzed by one-way ANOVA, followed by Tukey's test. *Asterisks* indicate a statistically significant difference ($p < 0.05$).

puncta were weaker than those in the ALG-2/Sec31A-negative puncta (Fig. 3*F*, *right panel*).

AnxA11 Is Required for Stabilization of Sec31A at the ERES—We then examined the effect of AnxA11 knockdown on Sec31A dynamics in live cells. Fig. 4*A* shows the efficiency of depletion by Western blot analysis. We observed a 70–80% decrease in AnxA11 expression with GAPDH as a loading control in cells transiently transfected with AnxA11-targeted siRNA duplexes, whereas expression of ALG-2 was suppressed to 10% by ALG-2-targeted siRNA duplexes in the parallel experiment. Following suppression of AnxA11 in the Sec31A-gfp cells, FRAP was performed (Fig. 4, *B* and *C*, and supplemental Movie S3), which revealed that the fluorescence recoveries of Sec31A-GFP puncta in AnxA11 knockdowns were faster than those in control siRNA-treated cells. Thus, the effect of ALG-2 knockdown on the FRAP curve (see Fig. 1, *C* and *D*) was recapitulated by knockdown of AnxA11. The result clearly reveals the requirement of AnxA11 for the stable association of Sec31A with the ERES.

Effects of ALG-2 and AnxA11 Knockdown on the Early Secretory Pathway—During the FRAP experiments, we noticed that Sec31A-GFP puncta appeared to be dispersed throughout the cytoplasm in the ALG-2 and AnxA11 knockdown cells. To evaluate the effects of suppression of ALG-2 or AnxA11 on the positioning of ERES, siRNA-transfected cells were immunostained with antibodies against Sec16A and a centrosome marker, γ-tubulin. Then, cells with a γ-tubulin-positive centrosome at the juxtanuclear region were chosen, and the distance between each Sec16A-positive punctum and the centrosome was measured in projected images of z-stacks encompassing the entire cell depth (Fig. 5*A*). As shown in the histogram (Fig. 5*B*), 30–40% of Sec16A-positive foci in the cells treated with control siRNA were concentrated in an area 5–10 μm from the centrosome. In the ALG-2- or AnxA11-knockdowns, Sec16A populations in this area were significantly decreased. Instead, Sec16A signals of the knockdowns were increased in regions distal to the centrosome (>15 μm). These observations are consistent with ALG-2 and AnxA11 having roles in the juxtanuclear positioning of Sec16A-positive structures.

To examine whether suppression of ALG-2 or AnxA11 affected protein trafficking in the early secretory pathway, we co-stained the knockdown cells with antibodies against ERGIC-53 and GM130 (Fig. 5*C*). ERGIC-53 is a lectin-type cargo receptor that continuously cycles between the ER, the

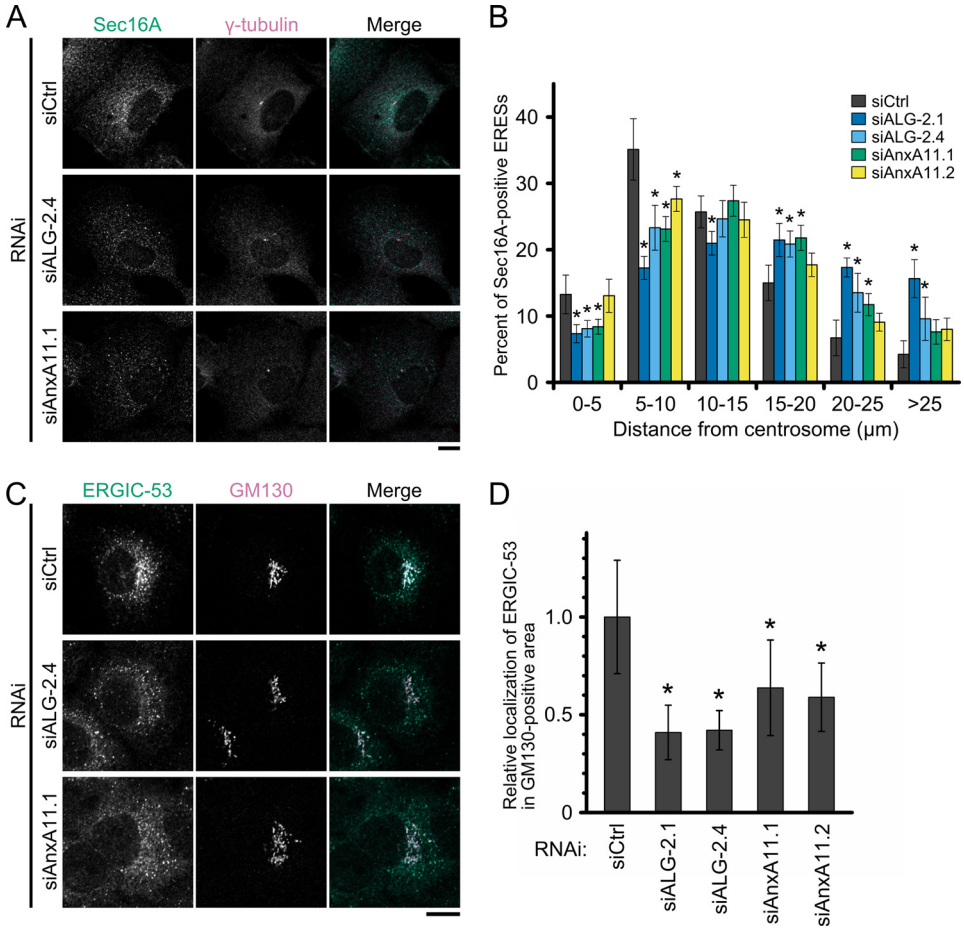

FIGURE 5. **Effects of ALG-2 or AnxA11 knockdown on intracellular positioning of the Sec16A-positive compartment and distribution of ERGIC-53.** *A,* representative confocal z-stack projection images of siRNA-treated HT1080 cells stained with antibodies against Sec16A and γ-tubulin. Cells were transfected with control (*siCtrl*), ALG-2 (*siALG-2.4*), or AnxA11 (*siAnxA11.1*) siRNAs, followed by fixation with 4% paraformaldehyde in phosphate buffer for 1 h at room temperature and permeabilization with 0.1% Triton X-100. Then cells were double-stained with antibodies against Sec16A and γ-tubulin. The images are superimpositions of serial optical sections taken through the whole thickness of the cell. The *right panel* in each row shows merged images with the pseudocolors as follows: *green* (Sec16A) and *magenta* (γ-tubulin). *Scale bar,* 10 μm. *B,* histogram of distribution of the Sec16A-positive compartments. Cells treated with siRNAs were processed in the same manner except for permeabilization with digitonin. The ratio of fluorescence intensity for Sec16A in individual Sec16A-positive compartments to that in whole Sec16A-positive compartments was calculated and grouped into bins of distances of 5 μm from the γ-tubulin-positive centrosome. Values and *bars* in each bin represent mean percentages ± 95% confidence intervals of cells treated with control (*siCtrl*: *gray*, $n = 15$), ALG-2 (*siALG-2.1*: *blue*, $n = 18$; *siALG-2.4*: *light blue*, $n = 18$), or AnxA11 (*siAnxA11.1*: *green*, $n = 17$; *siAnxA11.2*: *yellow*, $n = 18$) siRNAs from two independent experiments. The statistical significance of differences was analyzed by one-way ANOVA, followed by Tukey's test. Values with *asterisks* indicate a statistically significant difference from control ($p < 0.05$). *C,* confocal micrographs of siRNA-treated HT1080 cells stained with antibodies against ERGIC-53 and GM130. Cells transfected with indicated siRNAs were double-stained with antibodies against ERGIC-53 and GM130 as described in Fig. 3*E*. The *right panel* in each row shows merged images with the pseudocolors as follows: *green* (ERGIC-53) and *magenta* (GM130). *Scale bar,* 10 μm. *D,* quantitative analysis of ERGIC-53 distribution. The ratio of fluorescence intensity for ERGIC-53 in GM130-positive area to that in the whole cell in each cell transfected with the indicated siRNA was calculated. Values and *bars* represent relative mean values ± S.D. of cells treated with control (*siCtrl*: $n = 19$), ALG-2 (*siALG-2.1*: $n = 20$; *siALG-2.4*: $n = 20$) or AnxA11 (*siAnxA11.1*: $n = 22$; *siAnxA11.2*: $n = 16$) siRNAs. The statistical significance of differences was analyzed by one-way ANOVA, followed by Tukey's test. Values with *asterisks* indicate a statistically significant difference from control ($p < 0.01$). Representative data obtained from two independent experiments is shown.

ERGIC, and the cis-Golgi (40). Although the perinuclear Golgi stack pattern of staining for GM130 was not altered by ALG-2 or AnxA11 knockdown, the distribution pattern of ERGIC-53 was changed. Thus, in control siRNA-treated cells, ERGIC-53 showed clear overlap in the cis-Golgi area with GM130, although discrete spots were also visible outside the cis-Golgi. In contrast, ALG-2 or AnxA11 knockdown resulted in a decrease in ERGIC-53 staining in the perinuclear region, with a pronounced scattering of ERGIC-53-positive structures throughout the cytoplasm. As shown in Fig. 5*D*, the relative ratio of fluorescence intensity for ERGIC-53 in the GM130-positive area to that in the whole cell was significantly decreased in ALG-2- and AnxA11-knockdown cells compared with control siRNA-treated cells. These observations raise the possibility that ALG-2 and AnxA11 modulate a balance between the anterograde and retrograde transport of ERGIC-53 proteins and/or that the integrity of the ERGIC structure requires both ALG-2 and AnxA11.

We next used a temperature-sensitive variant (tsO45) of vesicular stomatitis virus glycoprotein (VSV-G) as a cargo molecule. VSV-G is a type I membrane protein, and tsO45 has an F204S substitution in the ectodomain (41). At the restrictive temperature, this mutant is misfolded and remains in the ER (42). However, at the permissive temperature, refolded and trimerized tsO45 glycoproteins are synchronously exported from the ER in a COPII-dependent manner and transported toward the Golgi apparatus. We established HT1080 cells stably expressing the tsO45 glycoprotein fused with SGFP2

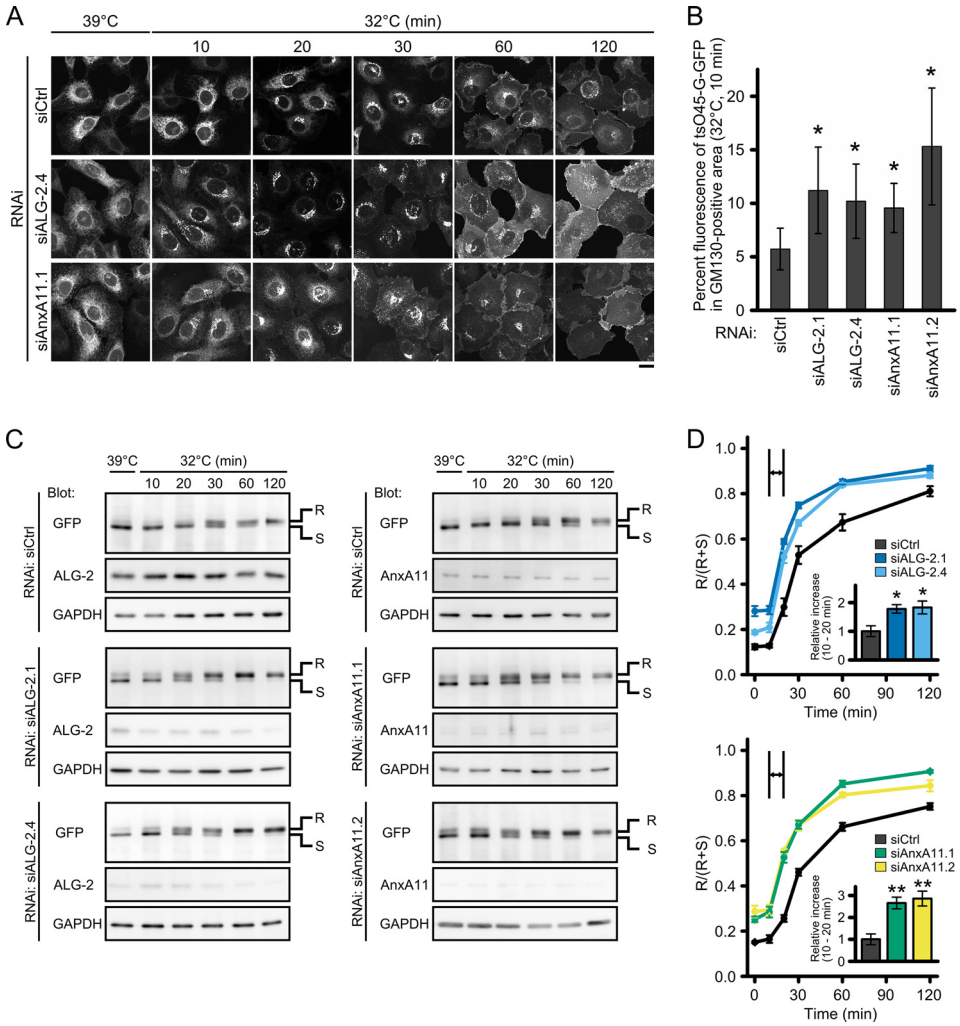

FIGURE 6. **Effects of ALG-2 or AnxA11 knockdown on the synchronous transport of temperature-sensitive vesicular stomatitis viral glycoprotein fused with SGFP2 (tsO45-G-GFP) from the ER.** *A*, confocal micrographs of siRNA-treated HT1080 cells stably expressing tsO45-G-GFP at indicated time points after the shift to the permissive temperature (32 °C). HT1080 cells stably expressing tsO45-G-GFP were transfected with indicated siRNAs, incubated at 39 °C for 24 h, and then shifted to 32 °C. After incubation for the indicated times, cells were fixed with 4% paraformaldehyde in phosphate buffer. Fluorescent signals of SGFP2 were observed under a confocal laser scanning microscope. *Scale bar,* 20 μm. Representative data obtained from at least three independent experiments are shown. *B,* quantitative analysis of tsO45-G-GFP transport to the cis-Golgi. HT1080 cells stably expressing tsO45-G-GFP were treated with indicated siRNAs and processed as described in *A*. Ten min after the shift to the permissive temperature, cells were fixed and stained with antibody against GM130 as described in Fig. 3*E*. The ratio of fluorescence intensity for tsO45-G-GFP in GM130-positive area to that in whole cell in each cell transfected with the indicated siRNA was calculated. Values and *bars* represent mean percentages and ± S.D. of cells treated with control (*siCtrl*: $n = 44$), ALG-2 (*siALG-2.1*: $n = 63$; *siALG-2.4*: $n = 60$) or AnxA11 (*siAnxA11.1*: $n = 52$; *siAnxA11.2*: $n = 62$) siRNAs. The statistical significance of differences was analyzed by one-way ANOVA, followed by Tukey's test. Values with *asterisks* indicate a statistically significant difference from control ($p < 0.01$). Representative data obtained from two independent experiments is shown. *C* and *D,* immunoblots of proteins in siRNA-treated HT1080 cells stably expressing tsO45-G-GFP at indicated time points after the shift to the permissive temperature (32 °C) and the kinetics of acquisition of Endo H resistance of tsO45-G-GFP. HT1080 cells stably expressing tsO45-G-GFP were transfected with indicated siRNAs, incubated at 39 °C for 24 h, and then shifted to 32 °C. After incubation at 32 °C for the indicated times, cells were lysed. Then the lysates were treated with Endo H and subjected to SDS-PAGE, followed by Western blotting using indicated antibodies. A representative blot obtained from at least three independent experiments is shown in *C* (*left panels*, siALG-2; *right panels,* siAnxA11). *R* and *S* indicate Endo H-resistant and -sensitive forms, respectively. Signals of R and S bands at each time were quantified, and the ratio of R to (R+S) was calculated and plotted by *black* (*siCtrl*), *blue* (*siALG-2.1*), *light blue* (*siALG-2.4*), *green* (*siAnxA11.1*), and *yellow* (*siAnxA11.2*) in *D* (*upper graph*, siALG-2; *lower graph*, siAnxA11). *Error bars* indicate S.E. (*upper graph*: *siCtrl*, $n = 8$; *siALG-2.1*, $n = 5$, *siALG-2.4*, $n = 3$; *lower graph*: *siCtrl*, $n = 7$; *siAnxA11.1*, $n = 4$; *siAnxA11.2*, $n = 3$). The relative rates of increase of R/(R+S) between 10 and 20 min are shown in the *inset*. The statistical significance of differences was analyzed by one-way ANOVA, followed by Tukey's test. Values with *asterisks* indicate a statistically significant difference from control (*, $p < 0.05$, and **, $p < 0.01$).

(tsO45-G-GFP) and examined the effects of suppression of ALG-2 or AnxA11 on the transport of tsO45-G-GFP. After incubation at the restrictive temperature (39 °C) for 24 h, tsO45-G-GFP accumulated throughout the ER in control cells as well as in ALG-2- and AnxA11-knockdown cells (Fig. 6*A*, *left-most panels*). In control cells, 20 min after the shift to the permissive temperature (32 °C), tsO45-G-GFP appeared to be exported from the ER and appeared as a tubule-vesicular network at the perinuclear area. At 30 min, the cells had a strong fluorescent signal at the Golgi complex, and at 60 min, tsO45-G-GFP was mainly found in dispersed, small punctate structures presumably for delivery to the cell membrane. At 120 min, most tsO45-G-GFP was seen at the cell surface. For ALG-2- and AnxA11-knockdown cells, at 20 min after release, most tsO45-G-GFP had already been transported to the Golgi. At 30 min, some cargoes were distributed throughout the cytoplasm in a vesicular pattern, and other fluorescent signals were detected at the cell surface. This pattern is similar to that in

control cells at 60 min after release. By 60 min, the majority of tsO45-G-GFP in the knockdown cells had reached the plasma membrane. Quantitation of the tsO45-G-GFP signal intensity at the GM130-positive area revealed that 10–15% of tsO45-G-GFP localized to the GM130-positive area 10 min after release in ALG-2- and AnxA11-knockdown cells, whereas only ~5% of tsO45-G-GFP was detected in control cells (Fig. 6*B*). These observations indicate a suppressive role for ALG-2 and AnxA11 in the synchronous transport of tsO45-G-GFP. We also monitored the ER-to-Golgi transport of tsO45-G-GFP by biochemically analyzing the kinetics of acquisition of endoglycosidase H (Endo H) resistance, which is a hallmark of delivery to the medial Golgi compartment (43). Fig. 6, *C* and *D,* shows that about 50% of the tsO45-G-GFP in control cells became Endo H-resistant by 30 min after release and that transport to the medial Golgi was increased to 70% at 120 min. In contrast, in ALG-2- and AnxA11-knockdown cells, acquisition of Endo H resistance was more than 50% at 20 min after release and reached a maximum at 60 min. The large differences between control cells and ALG-2- or AnxA11-knockdown cells correspond to the increased rate of acquisition of Endo H resistance from 10 to 20 min (slopes of the graphs in Fig. 6*D*, *insets*). These results show an acceleration of tsO45-G-GFP transport from the ER to the medial Golgi in ALG-2- and AnxA11-knockdown cells, further supporting a regulatory role of ALG-2 and AnxA11 in the early secretory pathway.

DISCUSSION

The COPII machinery forms flexible vesicles and plays a central role in exiting transport cargoes from the ER (3, 44). Many cytosolic proteins are recruited to the ERES through direct interaction with the COPII components or scaffolding proteins, which can modulate COPII activity and change the lipid composition of the ERES membrane (4, 45). In this study, we identified AnxA11 as a new modulator of the early secretory pathway. Annexins have been shown to participate in membrane organization and traffic (46), such as annexin A2 in Ca^{2+}-induced exocytosis (47, 48), and annexins A1 and A2 in the endocytic pathway (49–51). To our knowledge, this is the first study to report the involvement of a protein of the annexin family in the ER-to-Golgi transport.

Our FRAP study suggests that both AnxA11 and ALG-2 have a role in the stabilization of Sec31A at the ERES in living cells (Figs. 1 and 4). During preparation of this manuscript, la Cour *et al.* (52) reported that Ca^{2+}-bound recombinant ALG-2 increased recruitment of Sec13-Sec31A to artificial liposomes and stabilized complex formation of Sec13-Sec31A and Sec23 *in vitro*. Their conclusion obtained from an *in vitro* approach is consistent with our results showing that the stably associated population of Sec31A at the ERES was decreased by depletion of ALG-2 in HT1080 cells (Fig. 1, *C* and *D*). Interestingly, the loss of stably associated Sec31A was restored only by the major isoform of ALG-2 and not by the minor isoform of ALG-2 (Fig. 2, *B* and *C*), indicating that, in living cells, only the major isoform of ALG-2 has an essential role in the stabilization of Sec31A at the ERES. The major isoform of ALG-2 mediates the interaction of AnxA11 with Sec31A (Fig. 3, *B* and *C*), and the knockdown of AnxA11 elicits similar effects on the recycling kinetics of Sec31A but no change in the expression level of ALG-2 (Fig. 4). Based on these results, we propose that the recruitment of AnxA11 to the ERES by the adaptor function of ALG-2 is required for stabilizing Sec31A at the ERES in HT1080 cells. Sec31A has been shown to be phosphorylated by casein kinase II (CK2), and the phosphorylation appears to decrease association of Sec31A with the ER membrane (53). In this regard, there is the possibility that phosphorylated Sec31A might be increased in ALG-2- or AnxA11-knockdown cells.

In our immunofluorescence analysis, a subpopulation of cytoplasmic AnxA11 co-localizes with the Sec31A-positive ERES in HT1080 cells (Fig. 3, *E* and *F*). The cytoplasmic puncta labeled by the antibody against ALG-2 overlapped predominantly with Sec31A-positive structures (Fig. 3, *E* and *F*). However, the antibody for AnxA11 used in this study recognized the Sec31A/ALG-2-positive compartments to a lesser degree, which might be due to its antigenic site overlapping with the ALG-2-interacting N-terminal region. Other antibodies against the AnxA11 region outside the ALG-2-binding sites might be expected to give increased signal intensities for the Sec31A/ALG-2-positive ERES localization of endogenous AnxA11. The brighter puncta for AnxA11 did not overlap with Sec16A (data not shown), suggesting that the AnxA11-positive puncta are not in fact ERES. In addition to the function in the ERES, AnxA11 may have other roles in unidentified compartments in an ALG-2/Sec31A-independent fashion.

We have shown in this study that both ALG-2- and AnxA11-knockdown cells exhibit similar phenotypes in the early secretory pathway as follows: (i) dispersed distribution of ERES throughout the cytoplasm (Fig. 5, *A* and *B*); (ii) abnormal distribution of ERGIC-53 (Fig. 5, *C* and *D*); and (iii) accelerated transport of tsO45 VSV-G from the ER to Golgi apparatus (Fig. 6). These observations suggest that ALG-2 and AnxA11 function in the same process. Yamasaki *et al.* (15) reported (as data not shown) that there was no detectable difference in the rate of ER-to-Golgi trafficking of tsO45 VSV-G between control and ALG-2 knockdown HeLa cells, although in our study we observed a small increase in the rates of secretory trafficking in the ALG-2-knockdown HT1080 cells. This discrepancy might be due to variations in the expression level of AnxA11 between cell lines. Alternatively, the HT1080 cells stably expressing tsO45-G-GFP used in this study may maintain a moderate expression level of the cargo, which could give us a better time resolution to observe the detailed export of tsO45-G-GFP from the ER. Previously, the two roles of ALG-2/Ca^{2+} in ER-to-Golgi transport have been proposed based on the results of *in vitro* reconstitution analysis as follows: inhibition of homotypic fusion of COPII vesicles (17) and attenuation of COPII budding (52). The acceleration of tsO45-G-GFP transport in the ALG-2 knockdown cells is in good agreement with results obtained from the *in vitro* studies. More recently (after submission of this study), Helm *et al.* (54) reported that exogenous co-expression of the major isoform of ALG-2 and the Pro-rich region of Sec31A inhibits ER-to-Golgi transport of tsO45-G-GFP in normal rat kidney cells. In contrast, co-expression of the minor isoform of ALG-2, ALG-$2^{\Delta GF122}$ that binds Sec31A but lacks the adaptor function to bridge AnxA11 and Sec31A (Fig. 3*C*), fails to inhibit transport (54). This implies that AnxA11 may be

involved in the inhibitory effect of the complex between ALG-2 and the Pro-rich region of Sec31A in ER-to-Golgi transport.

We have also shown decreased distribution of ERGIC-53 in the cis-Golgi in ALG-2-knockdown cells as well as in AnxA11-knockdown cells (Fig. 5, *C* and *D*). To determine whether ERGIC-53 is re-localized to ERES by ALG-2 or AnxA11 knockdowns, we co-stained the knockdown cells with antibodies against ERGIC-53 and an ERES marker p125 (26). Unexpectedly, ERGIC-53 levels in the p125-positive compartments in the knockdown cells were similar to those in control cells (data not shown). This implies that ALG-2 and AnxA11 may not help to selectively sort ERGIC-53 into the COPII vesicles and to transport from the ERES, but it may have additional unknown roles in the early secretory pathway. Other specific cargoes and cargo receptors could be preferentially enriched in the transport vesicles by the COPII coat-stabilizing function of ALG-2/AnxA11 in response to Ca^{2+} mobilization, from where they would be synchronously transported to their final destinations after release of ALG-2/AnxA11 from the outer coat. In future work, proteomic analysis of COPII vesicles before and after Ca^{2+} mobilization may increase our understanding of the molecular mechanisms of AnxA11 function in the early secretory pathway.

Acknowledgments—We thank Haruna Yoshida for earlier works related to this study and Dr. Kiyotaka Hitomi (Nagoya University) and Dr. Terunao Takahara (Nagoya University) for their valuable suggestions. We also thank Dr. Katsuko Tani (Tokyo University of Pharmacy and Life Science) and Dr. Ikuo Wada (Fukushima Medical University School of Medicine) for providing materials.

REFERENCES

1. Bannykh, S. I., Rowe, T., and Balch, W. E. (1996) The organization of endoplasmic reticulum export complexes. *J. Cell Biol.* **135,** 19–35
2. Budnik, A., and Stephens, D. J. (2009) ER exit sites–localization and control of COPII vesicle formation. *FEBS Lett.* **583,** 3796–3803
3. Zanetti, G., Pahuja, K. B., Studer, S., Shim, S., and Schekman, R. (2012) COPII and the regulation of protein sorting in mammals. *Nat. Cell Biol.* **14,** 20–28
4. D'Arcangelo, J. G., Stahmer, K. R., and Miller, E. A. (2013) Vesicle-mediated export from the ER: COPII coat function and regulation. *Biochim. Biophys. Acta* **1833,** 2464–2472
5. Bi, X., Mancias, J. D., and Goldberg, J. (2007) Insights into COPII coat nucleation from the structure of Sec23.Sar1 complexed with the active fragment of Sec31. *Dev. Cell* **13,** 635–645
6. Stagg, S. M., Gürkan, C., Fowler, D. M., LaPointe, P., Foss, T. R., Potter, C. S., Carragher, B., and Balch, W. E. (2006) Structure of the Sec13/31 COPII coat cage. *Nature* **439,** 234–238
7. Fath, S., Mancias, J. D., Bi, X., and Goldberg, J. (2007) Structure and organization of coat proteins in the COPII cage. *Cell* **129,** 1325–1336
8. Berridge, M. J., Bootman, M. D., and Roderick, H. L. (2003) Calcium signalling: dynamics, homeostasis and remodelling. *Nat. Rev. Mol. Cell Biol.* **4,** 517–529
9. Beckers, C. J., and Balch, W. E. (1989) Calcium and GTP: essential components in vesicular trafficking between the endoplasmic reticulum and Golgi apparatus. *J. Cell Biol.* **108,** 1245–1256
10. Beckers, C. J., Plutner, H., Davidson, H. W., and Balch, W. E. (1990) Sequential intermediates in the transport of protein between the endoplasmic reticulum and the Golgi. *J. Biol. Chem.* **265,** 18298–18310
11. Pind, S. N., Nuoffer, C., McCaffery, J. M., Plutner, H., Davidson, H. W., Farquhar, M. G., and Balch, W. E. (1994) Rab1 and Ca^{2+} are required for the fusion of carrier vesicles mediating endoplasmic reticulum to Golgi transport. *J. Cell Biol.* **125,** 239–252
12. Chen, J. L., Ahluwalia, J. P., and Stamnes, M. (2002) Selective effects of calcium chelators on anterograde and retrograde protein transport in the cell. *J. Biol. Chem.* **277,** 35682–35687
13. Hay, J. C. (2007) Calcium: a fundamental regulator of intracellular membrane fusion? *EMBO Rep.* **8,** 236–240
14. Shibata, H., Suzuki, H., Yoshida, H., and Maki, M. (2007) ALG-2 directly binds Sec31A and localizes at endoplasmic reticulum exit sites in a Ca^{2+}-dependent manner. *Biochem. Biophys. Res. Commun.* **353,** 756–763
15. Yamasaki, A., Tani, K., Yamamoto, A., Kitamura, N., and Komada, M. (2006) The Ca^{2+}-binding protein ALG-2 is recruited to endoplasmic reticulum exit sites by Sec31A and stabilizes the localization of Sec31A. *Mol. Biol. Cell* **17,** 4876–4887
16. la Cour, J. M., Mollerup, J., and Berchtold, M. W. (2007) ALG-2 oscillates in subcellular localization, unitemporally with calcium oscillations. *Biochem. Biophys. Res. Commun.* **353,** 1063–1067
17. Bentley, M., Nycz, D. C., Joglekar, A., Fertschai, I., Malli, R., Graier, W. F., and Hay, J. C. (2010) Vesicular calcium regulates coat retention, fusogenicity, and size of pre-Golgi intermediates. *Mol. Biol. Cell* **21,** 1033–1046
18. Suzuki, H., Kawasaki, M., Inuzuka, T., Okumura, M., Kakiuchi, T., Shibata, H., Wakatsuki, S., and Maki, M. (2008) Structural basis for Ca^{2+}-dependent formation of ALG-2/Alix peptide complex: Ca^{2+}/EF3-driven arginine switch mechanism. *Structure* **16,** 1562–1573
19. Osugi, K., Suzuki, H., Nomura, T., Ariumi, Y., Shibata, H., and Maki, M. (2012) Identification of the P-body component PATL1 as a novel ALG-2-interacting protein by *in silico* and far-Western screening of proline-rich proteins. *J. Biochem.* **151,** 657–666
20. Kitaura, Y., Matsumoto, S., Satoh, H., Hitomi, K., and Maki, M. (2001) Peflin and ALG-2, members of the penta-EF-hand protein family, form a heterodimer that dissociates in a Ca^{2+}-dependent manner. *J. Biol. Chem.* **276,** 14053–14058
21. Okumura, M., Ichioka, F., Kobayashi, R., Suzuki, H., Yoshida, H., Shibata, H., and Maki, M. (2009) Penta-EF-hand protein ALG-2 functions as a Ca^{2+}-dependent adaptor that bridges Alix and TSG101. *Biochem. Biophys. Res. Commun.* **386,** 237–241
22. Maki, M., Suzuki, H., and Shibata, H. (2011) Structure and function of ALG-2, a penta-EF-hand calcium-dependent adaptor protein. *Sci. China Life Sci.* **54,** 770–779
23. Tomas, A., and Moss, S. E. (2003) Calcium- and cell cycle-dependent association of annexin 11 with the nuclear envelope. *J. Biol. Chem.* **278,** 20210–20216
24. Tomas, A., Futter, C., and Moss, S. E. (2004) Annexin 11 is required for midbody formation and completion of the terminal phase of cytokinesis. *J. Cell Biol.* **165,** 813–822
25. Arasaki, K., Taniguchi, M., Tani, K., and Tagaya, M. (2006) RINT-1 regulates the localization and entry of ZW10 to the syntaxin 18 complex. *Mol. Biol. Cell* **17,** 2780–2788
26. Shimoi, W., Ezawa, I., Nakamoto, K., Uesaki, S., Gabreski, G., Aridor, M., Yamamoto, A., Nagahama, M., Tagaya, M., and Tani, K. (2005) p125 is localized in endoplasmic reticulum exit sites and involved in their organization. *J. Biol. Chem.* **280,** 10141–10148
27. Shibata, H., Inuzuka, T., Yoshida, H., Sugiura, H., Wada, I., and Maki, M. (2010) The ALG-2-binding site in Sec31A influences the retention kinetics of Sec31A at the endoplasmic reticulum exit sites as revealed by live-cell time-lapse imaging. *Biosci. Biotechnol. Biochem.* **74,** 1819–1826
28. Ui-Tei, K., Naito, Y., Takahashi, F., Haraguchi, T., Ohki-Hamazaki, H., Juni, A., Ueda, R., and Saigo, K. (2004) Guidelines for the selection of highly effective siRNA sequences for mammalian and chick RNA interference. *Nucleic Acids Res.* **32,** 936–948
29. Inuzuka, T., Suzuki, H., Kawasaki, M., Shibata, H., Wakatsuki, S., and Maki, M. (2010) Molecular basis for defect in Alix-binding by alternatively spliced isoform of ALG-2 (ALG-$2^{\Delta GF122}$) and structural roles of F122 in target recognition. *BMC Struct. Biol.* **10,** 25
30. Ichioka, F., Takaya, E., Suzuki, H., Kajigaya, S., Buchman, V. L., Shibata, H., and Maki, M. (2007) HD-PTP and Alix share some membrane-traffic related proteins that interact with their Bro1 domains or proline-rich regions. *Arch. Biochem. Biophys.* **457,** 142–149
31. Shibata, H., Suzuki, H., Kakiuchi, T., Inuzuka, T., Yoshida, H., Mizuno, T.,

and Maki, M. (2008) Identification of Alix-type and non-Alix-type ALG-2-binding sites in human phospholipid scramblase 3: differential binding to an alternatively spliced isoform and amino acid-substituted mutants. *J. Biol. Chem.* **283,** 9623–9632
32. Osborn, M. (2006) in *Cell Biology: A Laboratory Handbook* (Celis, J. E., ed) 3rd Ed., pp. 549–555, Elsevier Academic Press, London, UK
33. Townley, A. K., Feng, Y., Schmidt, K., Carter, D. A., Porter, R., Verkade, P., and Stephens, D. J. (2008) Efficient coupling of Sec23-Sec24 to Sec13-Sec31 drives COPII-dependent collagen secretion and is essential for normal craniofacial development. *J. Cell Sci.* **121,** 3025–3034
34. Watson, P., Townley, A. K., Koka, P., Palmer, K. J., and Stephens, D. J. (2006) Sec16 defines endoplasmic reticulum exit sites and is required for secretory cargo export in mammalian cells. *Traffic* **7,** 1678–1787
35. Bhattacharyya, D., and Glick, B. S. (2007) Two mammalian Sec16 homologues have nonredundant functions in endoplasmic reticulum (ER) export and transitional ER organization. *Mol. Biol. Cell* **18,** 839–849
36. Iinuma, T., Shiga, A., Nakamoto, K., O'Brien, M. B., Aridor, M., Arimitsu, N., Tagaya, M., and Tani, K. (2007) Mammalian Sec16/p250 plays a role in membrane traffic from the endoplasmic reticulum. *J. Biol. Chem.* **282,** 17632–17639
37. Hughes, H., Budnik, A., Schmidt, K., Palmer, K. J., Mantell, J., Noakes, C., Johnson, A., Carter, D. A., Verkade, P., Watson, P., and Stephens, D. J. (2009) Organisation of human ER-exit sites: requirements for the localization of Sec16 to transitional ER. *J. Cell Sci.* **122,** 2924–2934
38. Tarabykina, S., Møller, A. L., Durussel, I., Cox, J., and Berchtold, M. W. (2000) Two forms of the apoptosis-linked protein ALG-2 with different Ca^{2+} affinities and target recognition. *J. Biol. Chem.* **275,** 10514–10518
39. Satoh, H., Shibata, H., Nakano, Y., Kitaura, Y., and Maki, M. (2002) ALG-2 interacts with the amino-terminal domain of annexin XI in a Ca^{2+}-dependent manner. *Biochem. Biophys. Res. Commun.* **291,** 1166–1172
40. Appenzeller-Herzog, C., and Hauri, H. P. (2006) The ER-Golgi intermediate compartment (ERGIC): in search of its identity and function. *J. Cell Sci.* **119,** 2173–2183
41. Gallione, C. J., and Rose, J. K. (1985) A single amino acid substitution in a hydrophobic domain causes temperature-sensitive cell-surface transport of a mutant viral glycoprotein. *J. Virol.* **54,** 374–382
42. Doms, R. W., Keller, D. S., Helenius, A., and Balch, W. E. (1987) Role for adenosine triphosphate in regulating the assembly and transport of vesicular stomatitis virus G protein trimers. *J. Cell Biol.* **105,** 1957–1969
43. Schwaninger, R., Beckers, C. J., and Balch, W. E. (1991) Sequential transport of protein between the endoplasmic reticulum and successive Golgi compartments in semi-intact cells. *J. Biol. Chem.* **266,** 13055–13063
44. Miller, E. A., and Schekman, R. (2013) COPII- a flexible vesicle formation system. *Curr. Opin. Cell Biol.* **25,** 420–427
45. Hughes, H., and Stephens, D. J. (2008) Assembly, organization, and function of the COPII coat. *Histochem. Cell Biol.* **129,** 129–151
46. Gerke, V., Creutz, C. E., and Moss, S. E. (2005) Annexins: linking Ca^{2+} signalling to membrane dynamics. *Nat. Rev. Mol. Cell Biol.* **6,** 449–461
47. Ali, S. M., Geisow, M. J., and Burgoyne, R. D. (1989) A role for calpactin in calcium-dependent exocytosis in adrenal chromaffin cells. *Nature* **340,** 313–315
48. Knop, M., Aareskjold, E., Bode, G., and Gerke, V. (2004) Rab3D and annexin A2 play a role in regulated secretion of vWF, but not tPA, from endothelial cells. *EMBO J.* **23,** 2982–2992
49. White, I. J., Bailey, L. M., Aghakhani, M. R., Moss, S. E., and Futter, C. E. (2006) EGF stimulates annexin 1-dependent inward vesiculation in a multivesicular endosome subpopulation. *EMBO J.* **25,** 1–12
50. Mayran, N., Parton, R. G., and Gruenberg, J. (2003) Annexin II regulates multivesicular endosome biogenesis in the degradation pathway of animal cells. *EMBO J.* **22,** 3242–3253
51. Morel, E., Parton, R. G., and Gruenberg, J. (2009) Annexin A2-dependent polymerization of actin mediates endosome biogenesis. *Dev. Cell* **16,** 445–457
52. la Cour, J. M., Schindler, A. J., Berchtold, M. W., and Schekman, R. (2013) ALG-2 attenuates COPII budding *in vitro* and stabilizes the Sec23/Sec31A complex. *PLoS One* **8,** e75309
53. Koreishi, M., Yu, S., Oda, M., Honjo, Y., and Satoh, A. (2013) CK2 phosphorylates Sec31 and regulates ER-To-Golgi trafficking. *PLoS One* **8,** e54382
54. Helm, J. R., Bentley, M., Thorsen, K. D., Wang, T., Foltz, L., Oorschot, V., Klumperman, J., and Hay, J. C. (2014) Apoptosis-linked gene-2 (ALG-2)/Sec31 interactions regulate endoplasmic reticulum (ER)-to-Golgi transport: a potential effector pathway for luminal calcium. *J. Biol. Chem.* **289,** 23609–23628